Figure 1: Rendered examples using our new BSDF.

Extending the Disney BRDF to a BSDF with Integrated Subsurface Scattering

by Brent Burley, Walt Disney Animation Studios

1 Introduction

We introduced a new physically based shading model on Wreck-It Ralph [Bur12], and we used this single, general-purpose BRDF on all materials (except hair). This model, which has come to be known as the Disney BRDF, is able to reproduce a wide range of materials with only a few parameters. For our next film, Frozen, we continued to use this BRDF unmodified, but effects like refraction and subsurface scattering were computed separately from the BRDF, and indirect illumination was approximated using point clouds. All of these effects were combined through ad hoc shading in an additive way.

Starting with Big Hero 6 in 2014, we switched from ad hoc lighting and shading to path-traced global illumination where refraction, subsurface scattering, and indirect illumination were all integrated in a single physically based framework. With path-traced global illumination, energy conservation becomes critical as non-energy conserving materials may amplify light and prevent the image from converging. The additive nature of ad hoc shading is generally not energy conserving given that the various components are redundant representations of the refracted energy. In order to ensure energy conservation, we extended our BRDF to a unified BSDF model where all such effects are accounted for in a consistent, energy-conserving way. Examples of our new model are shown in Figure 1.
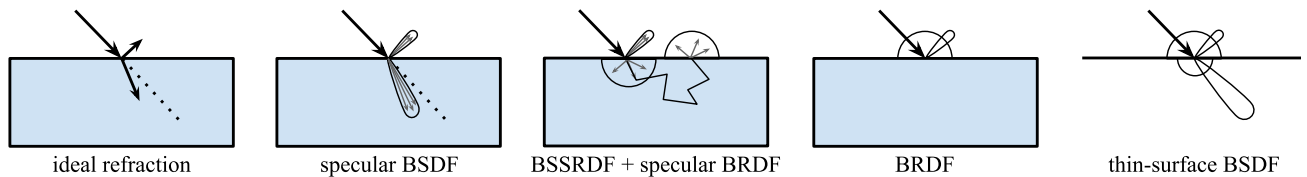

Figure 2: Various shading model representations of refracted energy.

1.1 Representations of refracted energy

When a ray hits a surface, the ray splits with some of the energy being reflected and some being refracted into the surface. The reflected portion of the ray is well described by a specular BRDF. However, the refracted portion of the ray, depending on the material, may continue through the object to be transmitted out the other side, or it may scatter internally and be re-emitted at some other point on the surface. These cases are traditionally handled as separate shading models as illustrated in Figure 2 and described below:

Ideal refraction: a smooth dieletric surface (such as glass) splits incident rays into reflected and refracted portions. The refracted rays change direction according to Snell's law, and the fraction of energy being reflected or refracted is described by the Fresnel equations. This is typically handled as a special purpose shader due to the delta distributions involved.

Specular BSDF: a rough surface scatters reflected and refracted rays at the surface boundary. This is commonly modeled using a microfacet BSDF, or *Bidirectional Scattering Distribution Function* [WMLT07]. Such a BSDF only describes specular scattering, and only at a single point; a ray refracting into a solid and exiting the other side would be represented as two BSDF scattering events.

BSSRDF + specular BRDF: refracted rays may be scattered multiple times below the surface, exiting at an arbitrary point away from the entrance point. The amount of energy being transmitted by such scattering between two locations and directions on a surface is described by a BSSRDF, or *Bidirectional Surface Scattering Distribution Function* [JMLH01]. For practicality, BSSRDF implementations typically employ a diffusion approximation that makes severe geometric assumptions.

BRDF: when the scatter distance is small compared to the rendering precision (e.g. smaller than a projected pixel), subsurface scattering can be effectively approximated by a diffuse BRDF. Such scattering is often assumed to be isotropic, i.e. Lambertian, though this is not the case for the Disney BRDF.

Thin-surface BSDF: when shading a thin, translucent surface (i.e. with no geometrically modeled internal volume), a thin-surface BSDF can represent both diffuse and specular reflection as well as diffuse and specular transmission.

Notably, each of these models is an approximation of the previous model. The thin-surface BSDF is thus an approximation of an approximation of an approximation of an approximation! Each of these approximations has their place, and our unified model incorporates aspects of all of them.

1.2 A unified scattering model

We would like to represent all forms of scattering within a unified model. The most general model perhaps would be a specular BSDF for the surface combined with a volumetric scattering model for the interior as shown in Figure 3 to the right. Such a model can reproduce all physical effects, though it is not always practical to do so; e.g. in this model surface color is derived solely from absorption during volume scattering though it would be sufficient and obviously more efficient to use a diffuse BRDF when the scatter distance is negligible.

Arguably, one might consider the BSSRDF as the most general unified representation of scattering since, mathematically at least, it fully describes all scattering between any two points and
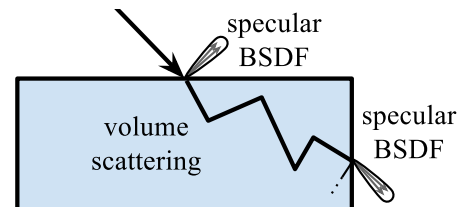

Figure 3: A specular BSDF reflects and refracts rays at the surface. Refracted rays are scattered and partially absorbed within the volume. When these rays reach the surface, they are scattered again according to another specular BSDF.
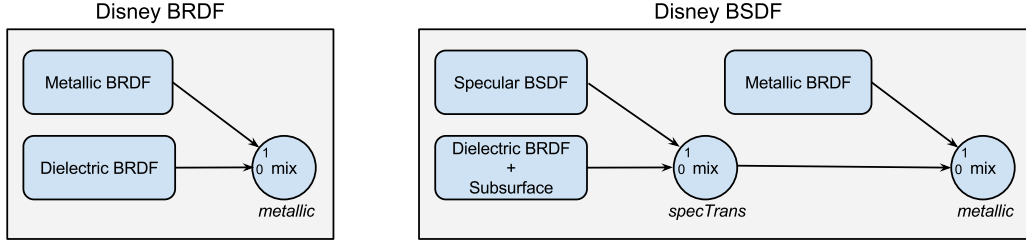
Figure 4: The Disney BRDF is a blend of metallic and dielectric BRDF models based on a *metallic* shader parameter. For our unified BSDF, we extend our dielectric BRDF with integrated subsurface scattering, and we blend in an additional specular BSDF based on a new *specTrans* parameter.

directions on a surface. However, the BSSRDF is an impractical representation for non-diffuse scattering given that the entry and exit points and directions must be known a priori, yet the exit point is often determined by tracing through the object after scattering at the surface. The general form of the BSSRDF presents a chicken and egg problem (or more technically, an example of the *searchlight problem* from radiative transport theory). The diffusion approximation of the BSSRDF, however, sidesteps this problem.

Rather than trying to use a single general model, our unified model is a *blend* of models, combining our existing BRDF with a specular BSDF and a subsurface scattering model. When the specular BSDF is selected and combined with a volume shader for the interior, we have the general scattering model of Figure 3, but we still have the more efficient approximations of the BRDF and subsurface diffusion available.

We refer to our unified model as the Disney BSDF though this isn't strictly correct given that our model includes subsurface scattering. Because of this, we more formally refer to our unified model as the *Disney BSDF with integrated subsurface scattering*.

2 Disney BSDF

We note that our Disney BRDF is already a blend of metallic and dielectric models. To support refraction, we extend this by blending an additional specular BSDF model as shown in Figure 4. A new parameter, specular transmission or *specTrans*, controls the blending. As seen in the figure, the metallic model takes precedence, but fractional blends of all three models are possible. If each constituent model is energy conserving, then the blend will be as well.

For thin surfaces, as suggested in Figure 2, special treatment is required. There's no internal volume present within which to perform subsurface scattering, so an approximation must be used. Also, for refraction, both the entering and exiting scattering events must be simultaneously simulated.

Each of these models is discussed in the following subsections. First, we recap the features of our Disney BRDF, then we describe the new additions.

2.1 Disney BRDF Recap

The Disney BRDF was largely based on observations of measured materials, primarily from the MERL 100 materials [MPBM03]. As such it was empirically inspired but follows an ad hoc construction where existing physically derived models didn't adequately reproduce measured material results.

Our BRDF includes two specular lobes: a microfacet reflection lobe with anisotropic roughness and an optional clearcoat reflection lobe. The microfacet reflection follows standard models [CT81, WMLT07]. The clearcoat lobe is isotropic and follows a similar but non-physical construction.
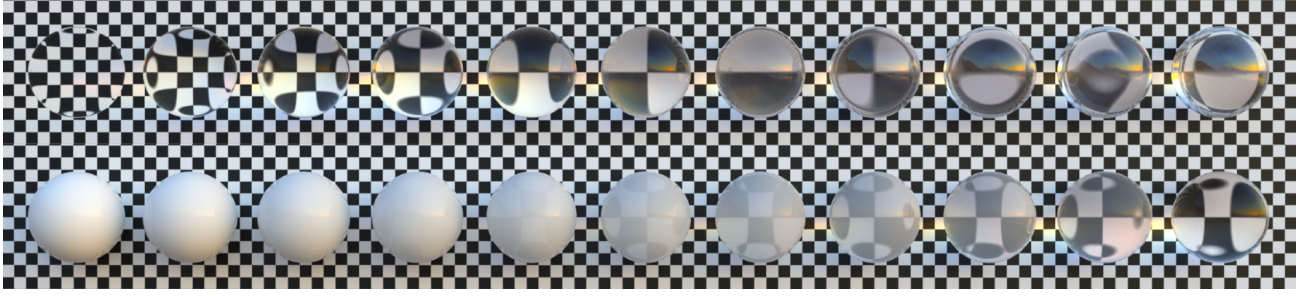
Figure 5: Top: Our specular BSDF with varying IOR from 1 to 2. (The leftmost sphere is shown at 1.02 rather than 1, otherwise it would be invisible.) Bottom: *specTrans* varying from 0 to 1 with IOR of 1.33.

Our BRDF diffuse response is directional (i.e. non-Lambertian). Specifically, the grazing retro-reflection response depends on the microfacet reflection roughness and ranges from darkening for smooth surfaces to brightening for rough surfaces. We also include an optional sheen component which adds grazing forward reflection. Both of these model observed effects in the measured materials which we presume to be caused by multiple-scattering effects between and through microsurface features.

Additionally, a completely separate (also directional and also roughness dependent) diffuse model is included that approximates subsurface scattering. This is still a BRDF, since no actual subsurface scattering is performed. This model is blended with the primary diffuse according to a user parameter. We have removed this model from our Disney BSDF in favor of true subsurface scattering for solid surfaces, though we retain it thin-surface shading.

The metallic portion of our BRDF simply kills all diffuse reflectance and sets the incident specular response to the specified *baseColor*. This *baseColor* parameter is shared with the dielectric (i.e. non-metallic) diffuse model and thus serves as an approximate estimate of the albedo for both models. We extend this interpretation of the *baseColor* parameter to our specular BSDF model.

While the Disney BRDF is not strictly energy conserving, for reasons discussed in Section 5.1, the parameters are defined in such a way as to produce plausible results that are energy conserving given plausible albedos which are typically much less than one.

2.2 Specular BSDF

Our specular BSDF directly extends the microfacet reflection lobe of our BRDF to refraction. Examples of our specular BSDF and blended specular transmission are shown in Figure 5.

We follow the derivation of Walter et al. [WMLT07]. Rays are refracted according to Snell's law, $\eta_i \sin \theta_i = \eta_o \sin \theta_o$ where η_i and η_o are the indices of refraction, or *IOR*s, of the two media at the refractive surface. Note that refraction only depends on the *ratio* of indices, $\eta = \eta_o/\eta_i$, commonly referred to as the *relative IOR*. When coming from air (where $\eta_i \approx 1.0003$ and typically assumed to be 1) the IOR and relative IOR are the same, but care must be taken to invert the value when refracting out of an object.

Snell's law describes the bending of rays, but less obviously, it also describes the spreading of rays. Specifically, the apparent radiance of a refracted ray will be scaled by η^2 which, as Veach shows [Vea97], is equivalent to the change in projected solid angle.

To derive the microfacet BSDF as the sum of a BRDF and BTDF, $f_s(\boldsymbol{i}, \boldsymbol{o}, \boldsymbol{n}) = f_r(\boldsymbol{i}, \boldsymbol{o}, \boldsymbol{n}) + f_t(\boldsymbol{i}, \boldsymbol{o}, \boldsymbol{n})$, Walter et al. first define the reflection and refraction half-vectors, applying Snell's law in

the refraction case:

$$h_r = \frac{i + o}{\|i + o\|}$$

$$h_t = -\frac{i + \eta o}{\|i + \eta o\|}$$

(1)

then apply three correction factors to 1) transform incident radiance onto the microsurface, 2) transform scattered radiance back to the macrosurface, and 3) account for the change in solid-angle measure, $\|\frac{\partial \omega_h}{\partial \omega_o}\|$. For refraction, a fourth factor is needed to account for the change in solid angle due to refractive spreading as mentioned above (a factor omitted by Walter et al.). Combining these factors results in:

$$f_r(i, o, n) = \frac{|i \cdot h_r|}{|i \cdot n|} \cdot \frac{|o \cdot h_r|}{|o \cdot n|} \cdot \frac{1}{(i \cdot h_r + o \cdot h_r)^2} \cdot F(i, h_r)G(i, o, h_r)D(h_r)$$

$$= \frac{F_r(i, h_r)G(i, o, h_r)D(h_r)}{4|i \cdot n||o \cdot n|}$$

(2)

$$f_t(i, o, n) = \frac{|i \cdot h_t|}{|i \cdot n|} \cdot \frac{|o \cdot h_t|}{|o \cdot n|} \cdot \frac{\eta^2}{(i \cdot h_t + \eta o \cdot h_t)^2} \cdot \frac{1}{\eta^2} \cdot (1 - F(i, h_t))G(i, o, h_t)D(h_t)$$

When the obvious terms are cancelled in f_r (noting that $i \cdot h_r = o \cdot h_r$) we have the familiar form of the microfacet BRDF. *Note:* these formulae are defined with respect to integration over the outgoing hemisphere. The BRDF is reciprocal but the BTDF is not, so care must be taken when choosing i and o. In particular, for path tracing from the camera, i would represent the view direction and o the light direction.

The $1/\eta^2$ spreading factor can usually be omitted without incident given that one usually sees *through* refractive solids where the factor and inverse factor cancel out. And doing so will avoid undesirable brightening when the camera sensor is placed in a medium other than air (e.g. under water); while it is not physically correct to place the camera under water without some sort of air-water transition, such a transition is not typically modeled. However, with bidirectional methods such as photon mapping, energy (photons) can be deposited inside a refractive medium, and correct integration requires that the factor be included. *Note:* when tracing photons (which have no solid angle), the spreading factor should not be used.

To this basic model we add:

- **clearcoat:** this is unchanged from our BRDF, contributing additional reflection and not participating in refraction.

- **surface absorption:** we multiply the refraction result by the square root of the surface color, which, after both the entering and exiting scattering events are accounted for, produces the expected albedo.

- **volumetric absorption:** we apply volumetric absorption based on the length of refracted paths through the solid.

- **sheen:** though non-physical, we include the sheen component from our BRDF. We note that the rough dielectric model presented by Walter et al. loses energy due to lack of microfacet inter-reflection/refraction and the sheen component can approximately compensate for it, and such compensation was deemed necessary by our artists. We discuss this issue further in Section 5.1.

Volumetric absorption parameterization: The Beer-Lambert law states that the transmittance T through a volume is exponential with respect to optical depth which can be represented as an absorption coefficient σ_a multiplied by distance d, thus $T = e^{-\sigma_a d}$. This is straightforward to
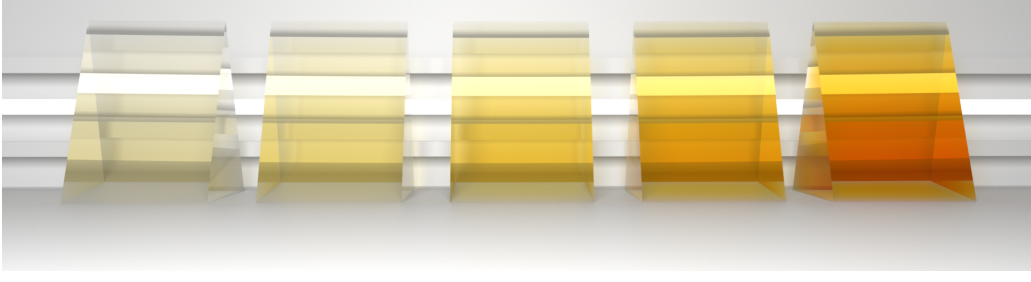
Figure 6: Volumetric absorption on refractive solids. The *transmittance* color is (1, 0.7, 0.1) with transmittance *atDistance* values of (16, 8, 4, 2, 1) from left to right on prisms with base thickness of 1.5 and IOR of 1.3.

implement but the absorption coefficient is unintuitive. Instead, we add two new parameters: a *transmittance* color, and corresponding *atDistance* factor from which we infer the absorption coefficient by inverting the transmittance equation: $\sigma_a = -(\log T)/d$. An example is shown in Figure 6.

2.3 Dielectric BRDF with integrated subsurface scattering

To extend our dielectric BRDF with subsurface scattering, we first refactor our diffuse lobe into directional *microsurface* effects and non-directional (i.e. Lambertian) *subsurface* effects, then we replace the Lambertian portion of the diffuse lobe with either a diffusion model or a volumetric scattering model. This preserves the microsurface effects, allowing our diffusion model to converge to the same result as the diffuse BRDF when the scatter distance is small.

For the Disney BRDF, our directional diffuse model was previously defined as:

$$f_d = \frac{baseColor}{\pi} \left(1 + (F_{D90} - 1)(1 - \cos\theta_l)^5\right) \left(1 + (F_{D90} - 1)(1 - \cos\theta_v)^5\right)$$

where
$$F_{D90} = 0.5 + 2 \, roughness \cos^2\theta_d$$

$$(3)$$

If we had used $F_{D90} = 0$, this would have been the standard Lambertian diffuse with smooth-surface Fresnel factors (using the Schlick Fresnel approximation here), but as discussed in our 2012 report this produces an unnaturally dark grazing response. So instead of going to 0 at grazing angles, i.e. when the light or view direction is 90 degrees from the surface normal, we limit the edge darkening to 0.5, and increase gain at retro-reflection by up to 2.5 times for maximally rough surfaces. The $\cos^2\theta_d$ factor smoothly isolates this gain to grazing retro-reflection. Though ad hoc, this shape and relationship to roughness were chosen based on observations of measured data.

To enable swapping out the Lambertian diffuse with subsurface scattering while retaining our rough-surface Fresnel factors and retro-reflective gain, we refactor our diffuse model as:

$$f_d = f_{Lambert} \left(1 - 0.5F_L\right) \left(1 - 0.5F_V\right) + f_{retro-reflection}$$
$$f_{Lambert} = \frac{baseColor}{\pi}$$
$$f_{retro-reflection} = \frac{baseColor}{\pi} R_R \left(F_L + F_V + F_L F_V \left(R_R - 1\right)\right)$$

where
$$(4)$$
$$F_L = (1 - \cos\theta_l)^5$$
$$F_V = (1 - \cos\theta_v)^5$$
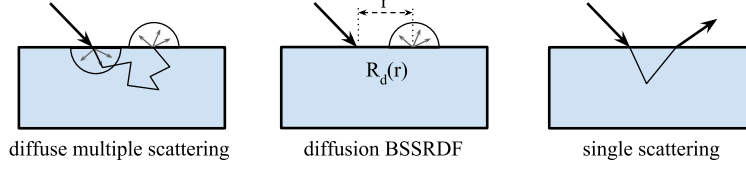$$R_R = 2 \, roughness \cos^2\theta_d$$

6

Figure 7: The *diffusion BSSRDF* model approximates diffuse multiple scattering, often depending only on distance r between surface points. This can be augmented with single scattering which assumes ideal refraction.

Our sheen component additionally models grazing microsurface transmission as $sheen \cdot (1 - \cos\theta_d)^5$, optionally tinted towards *baseColor* according to the *sheenTint* parameter. Given that this is already a separately added component, it is unaffected when swapping out the Lambertian diffuse component with subsurface scattering.

2.4 Subsurface diffusion

Subsurface diffusion in the form of the dipole model was introduced to graphics in a seminal paper by Jensen et al. [JMLH01]. In this work, it is assumed that the surface bounds a flat, semi-infinite slab—a reasonable assumption when the scattering distance is small with respect to surface curvature and thickness. The energy propagating between two points is defined using radiative transport theory and the multiple scattering diffusion component is approximately determined with single scattering separately integrated, illustrated in Figure 7. Subsequent work has improved this approximation, but has retained the geometric assumptions and increased the cost of evaluation [dI11, HCJ13].

Artistic control can be a challenge with diffusion models. Artists prefer to specify the diffuse albedo and mean multiple scattering distance, and the radiative transport scattering coefficients must therefore be inferred by inverting the diffusion equation [JB02]; such "albedo inversion" must typically done with iterative or tabulated methods, both of which can have trouble with high albedos. Another challenge is that diffusion profiles are often too blurry given that they typically only model multiple scattering, leading to the use of two or more profiles combined in an ad hoc manner.

For our diffusion model, we take a different approach. First, we observe through Monte Carlo simulation that for typical scattering parameters the diffusion profile *including* single scattering is well-approximated by a sum of two exponentials as shown in Figures 8 and 9. Based on simulating and fitting a range of scattering parameters, we chose the following prototypical shape for our diffusion profile:

$$R_d(r) = \frac{e^{-r/d} + e^{-r/(3d)}}{8\pi\,d\,r} \tag{5}$$

To evaluate the diffusion contribution, incident radiance must be integrated over the entire surface. Notably, when integrated over the hypothetical infinite surface over which diffusion models are defined, our profile is intrinsically normalized:

$$\int_0^{2\pi} \int_0^{\infty} R_d(r)\,r\,dr\,d\phi = 1 \tag{6}$$

and thus we refer to our profile as *normalized diffusion*. Because our profile is normalized, we can achieve our desired diffuse color simply by multiplying the integrated result at the end by *baseColor*, avoiding the need for albedo inversion and guaranteeing consistency with our diffuse BRDF. We expose the parameter d directly to artists as *scatterDistance* with components for red, green and blue. When *scatterDistance* is 0, we simply revert to our diffuse BRDF. A production result image is shown in Figure 10, and the effect of varying *scatterDistance* is shown in Figure 11.

In addition to being more consistent and convenient, Christensen [CB15] showed that our profile is also more accurate compared to state-of-the-art diffusion profiles, even when they are augmented with
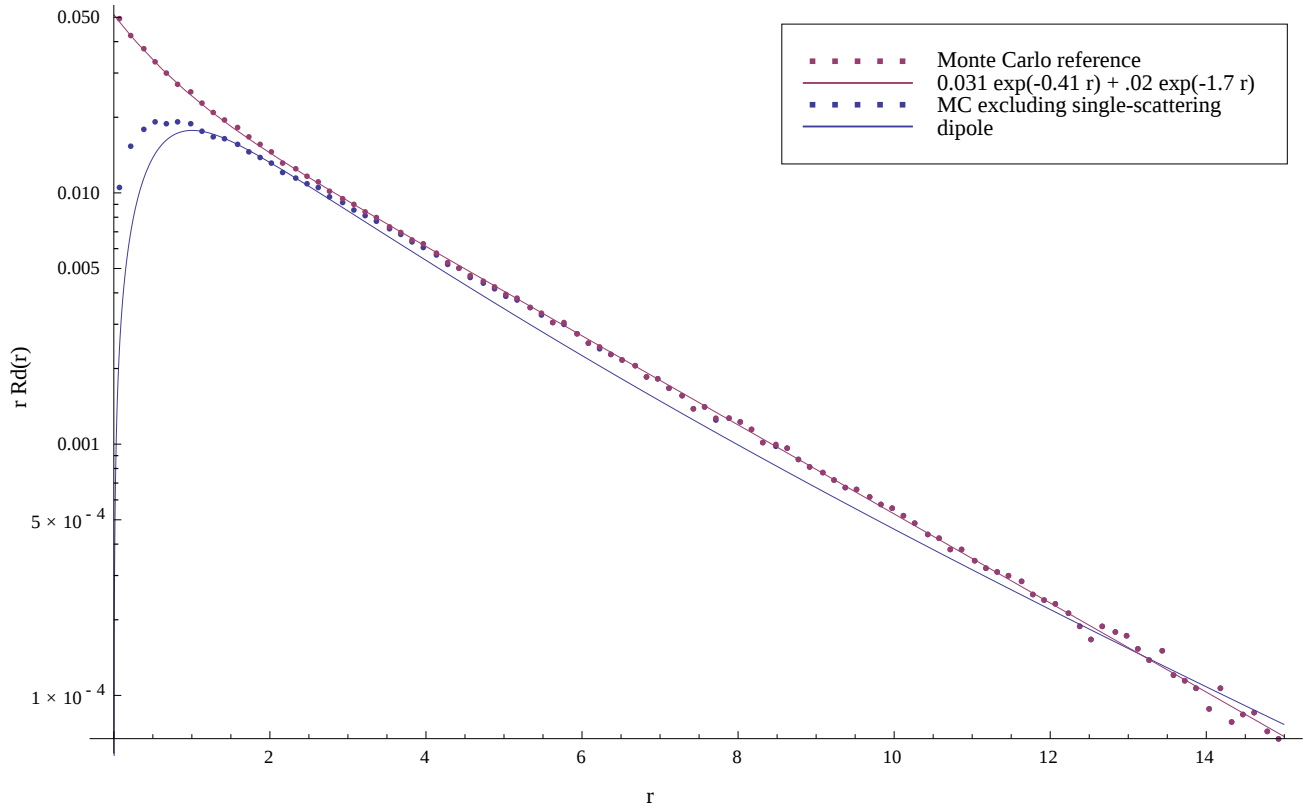
Figure 8: Monte Carlo diffusion simulation for *skin1.r* from [JMLH01] with exponential fit compared with Dipole.
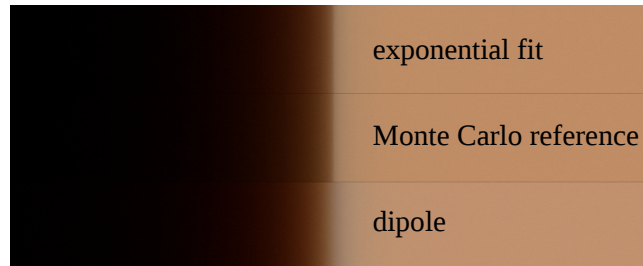

Figure 9: Monte Carlo diffusion rendering of *skin1* at a shadow boundary compared with exponential fit and dipole diffusion. The exponential fit is indistinguishable from the reference whereas the dipole model is visibly blurry with an objectionable cyan band, both frequent complaints of artists.

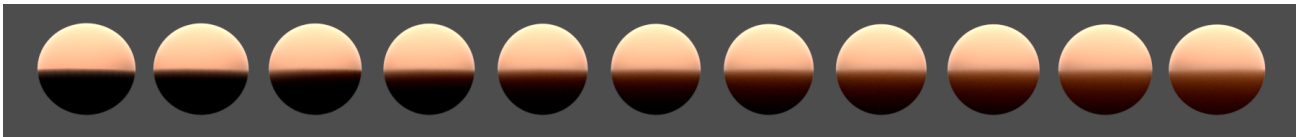Figure 10: Image from Big Hero 6 rendered using our normalized diffusion subsurface model. Image ©Disney 2014.

Figure 11: Unit spheres rendered with *scatterDistance* varying from $(0.0, 0.0, 0.0)$ to $(0.5, 0.25, 0.125)$. The spheres are lit by a furnace and artificially shadowed below the horizon to emphasize the shadow boundary. Notably, the first sphere uses the diffuse BRDF approximation, showing that the diffusion converges to a consistent result.
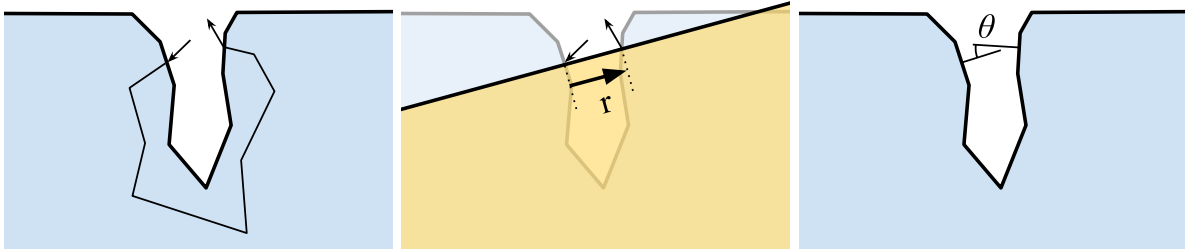
Figure 12: Left: a surface cavity is illustrated with a representative scattering path. Middle: the diffusion approximation views the surface as flat, depending only on the distance between the points and overestimating the energy transferred. Right: we use the angle between normals of opposing surfaces to reduce the diffusion amount.

single scattering (which is implicitly included in our profile). Christensen derived simple equations to relate our parameter d to the physical mean free path from radiative transport theory. Such relations facilitated comparison with other profiles, and also allowed our profile to be used as a drop-in replacement.

Our profile is also more efficient. In addition to having a relatively simple form and avoiding a separate integration for single scattering, it can be directly and analytically importance sampled as the CDF and inverse CDF are trivially derived. *Note:* to do so requires sampling each exponential lobe separately which is not a problem; three profiles are typically required for red, green and blue, and thus six lobes must be sampled which can be easily combined with multiple-importance sampling.

Though our diffusion profile is efficient to evaluate and matches the Monte Carlo reference well, there are still several drawbacks:

- The semi-infinite slab assumption creates artifacts when the scattering distance is large, as evident in Figure 13.

- Surface cavities are a particular problem, illustrated in Figure 12 which we partly address by fading out the diffusion result as the surfaces become opposing.

- Diffusion tends to blur out small surface details because the surface normals are ignored by the diffusion profile.

- Sampling can be difficult and expensive. Diffusion integration requires distributing samples over the entire surface with known density, preferably proportional to the diffusion profile. We can generate such samples within a plane, but projecting this density through a solid can oversample some parts of the surface and undersample others. Using MIS between multiple planes [KKCF13] helps prevent undersampling but oversampling is still a problem. Each plane sample also requires ray probing to find surface hits, and if there are multiple intersections we build a conditional CDF based on the distance to each point, then stochastically choose a point to sample. The per-sample cost is substantial.

2.5 Path-traced subsurface scattering

We are now finding that path-traced subsurface scattering can be a practical alternative that is nearly as efficient as diffusion while avoiding most of the artifacts. Figure 13 illustrates artifacts that can occur with diffusion on complex geometry, artifacts which go away with path-traced subsurface scattering. And Figure 14 shows that path-traced subsurface can be a practical production solution. In that image from Frozen Fever, the snowman, *Marshmallow*, is made up of both ice and snow which integrate seamlessly with path tracing. Previously, artists struggled with integrating ice with diffusion-rendered snow, and avoiding artifacts, especially in crevices.
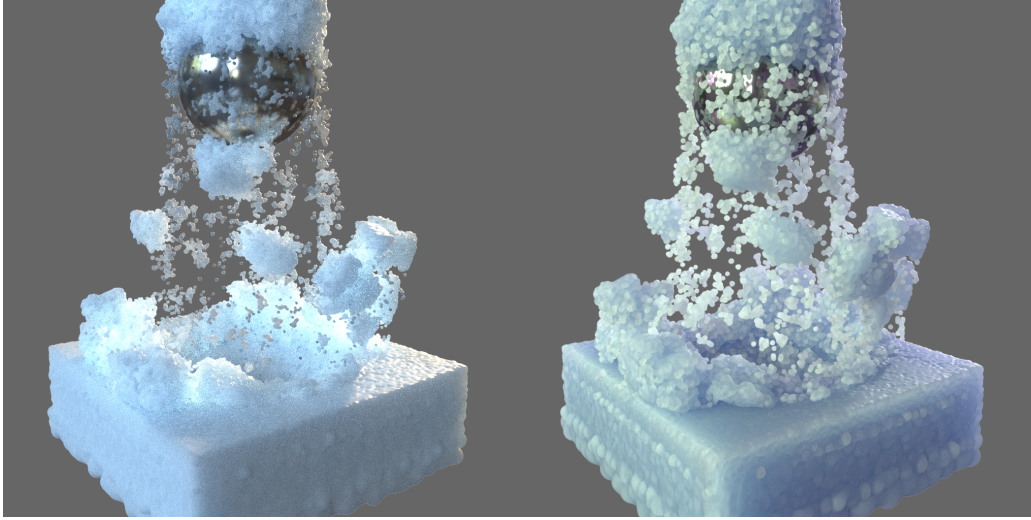
Figure 13: Left: image rendered with subsurface diffusion. Small droplets are visibly too dark, and areas with complex folds are too bright, appearing emissive; both artifacts are due to integrating over a surface area that differs from the infinite slab assumed by diffusion models. Right: path-traced subsurface avoids these artifacts.

Figure 14: Image from *Frozen Fever*, rendered using path-traced subsurface. Image ©Disney 2015.
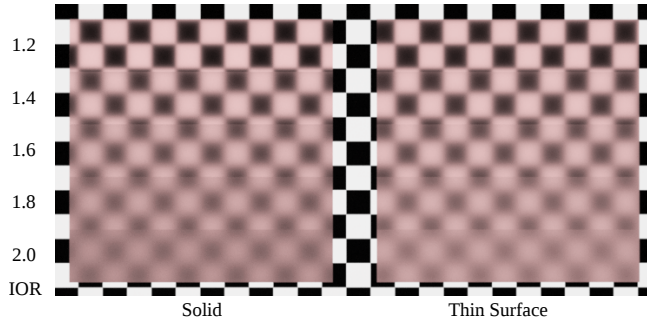
Figure 15: Left: Geometrically thin solid with IOR varying in strips, each with roughness of 0.35. The transmissive blurring obviously increases with IOR. Right: Thin-surface BSDF approximation with transmission roughness scaled by $(0.65\eta - 0.35)$ to approximately match.

2.6 Thin-surface BSDF

For thin, translucent surfaces, we simulate both the entrance and exit scattering events at a single shading point as a combination of specular and diffuse transmission, controlled by our *specTrans* and *diffTrans* parameters in a manner analogous to our solid surface shader. The *specTrans* parameter blends between a fully diffuse model and a fully specular model. The *diffTrans* parameter transfers energy from the diffuse reflection lobe to the diffuse transmission lobe; a value of 1 makes the front and back lobes equal, and the value can be increased up to 2 to give all the energy to transmission. As with solids, the micro-surface diffuse effects, sheen and diffuse retro-reflection, are included in the thin-surface front-side diffuse model and are unaffected by diffuse transmission. Additionally, we retain the subsurface approximation from our original BRDF as an alternate diffuse shape. This was originally controlled by the *subsurface* parameter which we have renamed *flatness* to avoid confusion with true subsurface scattering.

We observe that bending due to refraction on thin surfaces approximately cancels, and thus we model specular transmission using a microfacet distribution equivalent to our BRDF specular lobe but reflected to the other side. However, this is not entirely satisfactory as the effective transmission roughness should depend on the IOR since refractive bending can either amplify or attenuate the transmissive blurring. Indeed, if $\eta = 1$ then rays will pass right through the microfacets unperturbed. A better match can be achieved by scaling the roughness (for transmission only) based on the IOR as illustrated in Figure 15.

We approximate thin-surface diffuse transmission with an isotropic lobe. This is justified by the assumption that transmission due to subsurface scattering is isotropic. Our diffuse and specular transmission lobes are admittedly simplistic. Potential improvements are discussed in Section 5.2.

3 Disney BRDF Revisited

3.1 Schlick Fresnel

For our BRDF, we used the Schlick Fresnel approximation [Sch94], $F_{Schlick}(\theta_i) = F_0 + (1 - F_0)(1 - \cos\theta_i)^5$. This was efficient and reasonably accurate for plausible IOR values. However, care must be taken when used for refraction, especially when refracting out of an object where angles beyond the critical angle, $\theta_c = \sin^{-1}\eta$, should result in total internal reflection.

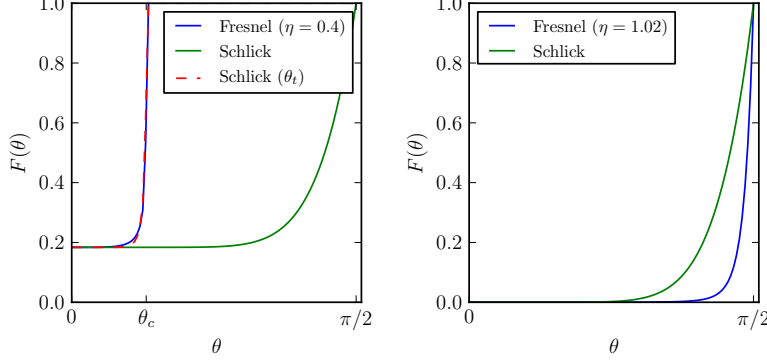An easy way to adjust the Schlick approximation to account for the critical angle is to simply use

Figure 16: Errors in Schlick approximation with refraction. Left: when the $\eta < 1$, as when refracting out of a solid, the Schlick approximation erroneously ignores the critical angle, θ_c; evaluating using the refracted angle θ_t rather than the reflected angle restores the approximation. Right: when the relative index of refraction is near 1, the error in the Schlick approximation becomes large.

the refracted angle $F(\theta_t)$ instead of the incident angle when the relative IOR is less than 1:

$$F_0 = \left(\frac{1-\eta}{1+\eta}\right)^2$$

$$\cos^2 \theta_t = 1 - \frac{1 - \cos^2 \theta_i}{\eta^2} \tag{7}$$

$$F_{Schlick|\eta<1}(\theta_i, \eta) = \begin{cases} F_0 + (1 - F_0)(1 - \cos \theta_t)^5 & \text{if } \cos^2 \theta_t > 0 \\ 1 & \text{otherwise} \end{cases}$$

This correction is illustrated in Figure 16, left. Another source of error with the Schlick approximation, illustrated in Figure 16, right, occurs when the relative IOR is close to 1. This can occur when viewing an embedded solid, such as ice from under water ($\eta = 1.33/1.31 \doteq 1.02$). As a result, the specular highlight on the ice can be nearly 40 times too bright. In the limit, surface reflection should disappear as the relative IOR goes to 1, yet Schlick reflection remains the same.

For our BSDF, given that we already need to compute the refracted direction, and considering the significant error introduced near $\eta = 1$, we abandoned the Schlick approximation in favor of the exact (unpolarized, dielectric) Fresnel equation:
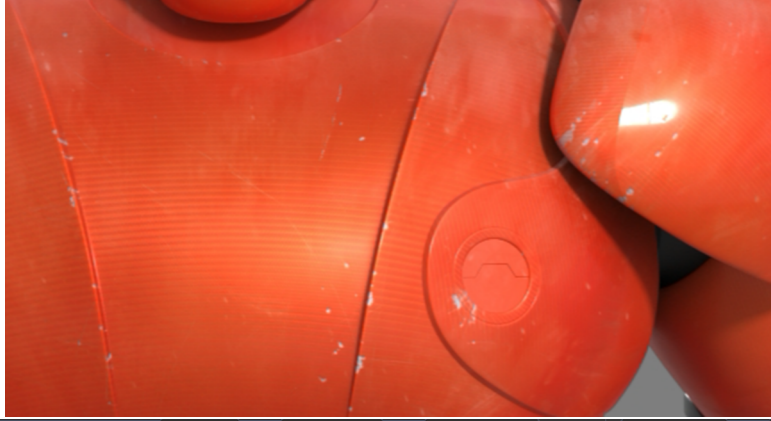
$$F(\theta_i, \eta) = \begin{cases} \frac{1}{2}\left[\left(\frac{\cos \theta_i - \eta \cos \theta_t}{\cos \theta_i + \eta \cos \theta_t}\right)^2 + \left(\frac{\cos \theta_t - \eta \cos \theta_i}{\cos \theta_t + \eta \cos \theta_i}\right)^2\right] & \text{if } \cos^2 \theta_t > 0 \\ 1 & \text{otherwise} \end{cases} \tag{8}$$

We observe that since we are already computing θ_t, the additional cost of computing the full Fresnel equation is negligible.

For our metallic BRDF, diffuse lobe, clearcoat, and specular tint, we still use the Schlick approximation. We discuss revisiting our metallic model later in section 5.3.

3.2 Index of Refraction

For our BRDF we avoided exposing IOR directly as a parameter because it was considered unintuitive for artists. Instead, we inferred the IOR from the Fresnel equation at normal incidence, controlled by the familiar *specular* parameter but rescaled to a plausible range: $F_0 = 0.08 \, specular$. The implied IOR was thus $\eta = 2/(1 - \sqrt{F_0}) - 1$ though this value was never needed given our use of the Schlick approximation. The normal range for *specular* of $[0, 1]$ thus corresponded to an IOR range of $[1, 1.8]$, with 0.5 notably corresponding to an IOR of 1.5, a typical value for polyurethane.

13

Figure 18: Production example from Big Hero 6 of layered material using parameter blending, with parameter values shown. Image ©Disney 2014.

+ -	mask	metallic	roughness	anisotropic	specularTint	sheen	sheenTint	clearcoat	clearcoatGloss	specTrans	ior	scatrDistR	scatrDistG	scatrDistB
1 ▸		0.39	0.475	0.4	0.5	0.1	0.5	1.75	1.0	0.0	1.2	0.0	0.0	0.0
2 ▸	NOarmorgridMask ## * armorGrid[0]->expand(.5,7)	0.44	0.28	0.325										
3 ▸	armorDecals	0.455	0.32	0.0				1.0	1.0					
4 ▸	~wearTestMask	0.42	0.5					0.4	0.3					
5 ▸	(armorGrid[2] * ~wearTestMaskB) * damagedMask	0.8	0.3	0.4				0.0	0.1		1.65			
6 ▸	~wearTestMaskB[0] * damagedMask	0.875	0.65					0.0	0.0		1.235			
7 ▸	dustMask * dustMult	0.0	0.7	0.0		1.2					1.15			

For our BSDF, the IOR controls the degree of bending for refractive solids. To ensure energy conservation and plausibility, we require the same IOR to be used for reflection and refraction, and our artists now find it intuitive to control this with the IOR directly when they understand the plausible range. IOR values range from 1 for air to perhaps 2 for the vast majority of materials with most common materials in the 1.3–1.6 range and only a few extremely dense materials going beyond 2 (e.g. for diamond, $\eta \approx 2.5$), and [Pol08]. Artists merely need to understand that the plausible range is [1, 2] with common materials close to 1.5.
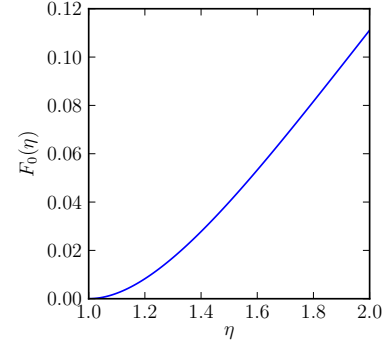
A secondary goal of our BRDF was choosing linear or perceptually linear parameters to enable parameter blending, so that an equal blend of parameters would reasonably approximate an equal blend of materials. Fortunately, the IOR is reasonably linear with respect to the incident reflectance in the plausible range as seen in Figure 17. This means that a mix of two IOR values will produce almost the same result as the interpolated incident reflectance.

Figure 17: Incident reflectance F_0 vs. IOR is nearly linear in the common material range of [1.3, 1.6].

3.3 Smith G

As we noted in a 2014 addendum to our 2012 notes [Bur12] and restate here, based on Heitz' analysis [Hei14] we eliminated our ad hoc remapping of the Smith G roughness for our primary specular lobe, and we adopted Heitz' anisotropic form. The result is obviously better for metals and arguably better for non-metals, though the G term still loses energy, an issue we discuss further in Section 5.1. Our clearcoat specular lobe remains unmodified.

3.4 Parameter blending with pass-through

In our 2012 notes, we described a user interface for layered materials where each layer defines a specific set of parameter values and then these layers are "parameter blended" according to spatially varying

Figure 19: Production still from Big Hero 6. Image ©Disney 2014.

masks. The blended values produce plausible in-between material results and avoid expensive multi-BRDF integration. This turned out to be very intuitive for artists and remains our sole interface for material specification.

Originally, we had 10 parameters in our reflectance layers. With the BSDF, we now have 12 for solids, adding *specTrans* and *scatterDistance*, or 13 for thin surfaces, adding *specTrans*, *diffTrans*, and *flatness* as previously described. To make this less cumbersome when adding non-translucent layers, we added a new feature to our UI, parameter pass-through.

With parameter pass-through, artists can leave entries in the table blank. During parameter blending, when a blank is encountered, the previously blended result will be held. This simple change has greatly improved the usability of the layering interface.

A production example of a layered material is shown in Figure 18 along with the UI and values used.

4   Production Results

Our new BSDF was used on every surface in Big Hero 6 except for hair, and refractive effects of all types were used extensively. In the production still shown in Figure 19, Baymax uses thin-surface shading with a blend of diffuse and specular transmission, convincingly conveying that he is made of inflated vinyl. Thin-surface shading was also used variously for cloth and paper. Windows were typically modeled as refractive solids. Figure 20 shows an additional still with several refractive solids. All skin and many solid objects such as plastic were rendered using normalized diffusion.

Rendering of the images in Big Hero 6 used multi-bounce path tracing, with the full BSDF response on every bounce. The BSDF proved to be robust and easy to control, with predictable results in all lighting conditions. In particular, artists found it easy to seamlessly blend between various refractive effects, and our new parameter pass-through UI made layering especially easy, with artists reaching a new level of productivity. The BSDF also proved efficient enough to enable an average to 10.5 billion shader evaluations per frame.

Figure 20: Production still from Big Hero 6. Image ©Disney 2014.

Figure 21: Left: A rough glass sphere (IOR=1.5, roughness=0.25) is rendered in a furnace and exhibits energy loss at grazing angles. Right: Adding sheen with a strength of 4.0 approximately replaces the energy loss.

5 Future

5.1 Energy conservation

The principle of energy conservation in reflectance modeling is generally understood to mean that a surface cannot reflect more energy than it receives, however it is just as important that a surface not *lose* energy. Of course, surfaces do absorb energy which results in their apparent color or albedo, but if a surface is modeled without absorption then ideally all energy should be reflected.

The so-called furnace test is often used to test energy conservation. When rendered in an environment with uniform radiance, an energy-conserving material with albedo 1 will "disappear" whereas a non-conserving material will either appear too light or too dark, or both, depending on viewing angle. Heitz noted that microfacet models typically do not model multiple scattering and thus do not pass the furnace test [Hei14]. Energy that is shadowed by the microfacet G factor is lost. Heitz proposed the "weak white furnace test" as a method for validating microfacet models, that they at least conserve energy up to the first scattering event and only lose energy from multiple scattering between microfacets. In the weak test, the shadowing term is omitted which represents measuring radiance after the first scattering event but before scattered rays are shadowed by the microsurface. The Smith shadowing function is shown to pass such a test, however it fundamentally still loses energy.

The effect of microfacet energy loss can be observed in Figure 21 where a rough glass sphere appears dark on the edge when rendered in a furnace. Multi-bounce path tracing is used for internal reflection.

This isn't just a theoretical problem: this image is representative of what rough glass looks like when rendered with existing microfacet models in an evenly lit environment, that it looks unnaturally dark on the edges.

We note anecdotally, and show in Figure 21, that adding sheen can make the glass sphere almost perfectly pass the furnace test. This is not to say that our sheen model is accurate, and in fact it has the wrong shape for other roughness values, but rather the *motivation* for having it is justified. The motivation for our diffuse retroreflection is similarly justified.

For future work, we would like to revisit our retroreflection and sheen components and potentially replace them with components that correctly conserve energy. For example, recent work by Jakob et al. [JdJM14] proposes a diffuse correction term to replace lost energy from microfacet interreflection.

5.2   Better thin-sheet model

As we previously discussed, our thin-sheet model is overly simplistic and we would like to revisit our formulation. Recent work proposes more rigorously defined and experimentally validated models for both specular and diffuse transmission through thin sheets [GQP15, PdMJ14].

5.3   Better metallic model

Our metallic model differs from true metallic response in that we use the Schlick Fresnel approximation. The correct Fresnel equations for conductors have a more complex shape that depends on an additional material parameter, the material's spectral *absorption coefficient*, k. The relationship between IOR, the absorption coefficient, and the resulting color is unintuitive, and arbitrary parameter combinations are implausible.

Recent work by Gulbrandsen [Gul14] promises artist-friendly control by reparameterizing the (spectral) IOR and absorption coefficients via direct specification of incident and edge colors, a parameterization we hope to investigate with our artists.

6   Conclusion

We have presented our new Disney BSDF, an extension of our BRDF with integrated refraction and subsurface scattering, and we have described our novel diffusion profile which has efficiency, accuracy, and controllability advantages. We have shown production examples and discussed implementation issues and limitations.

In conclusion, we would like to emphasize that we believe the value of our model comes more from our unified approach—having a single model with a intuitive, minimal set of parameters that can be used for nearly all materials—and less from the specific constituent parts. We will continue to improve the robustness or plausibility of the model and extend it as our needs dictate, but we remain committed to the generality and simplicity of our approach.

7   Acknowledgements

References

[Bur12]   Brent Burley. Physically-based shading at Disney, course notes, revised 2014. In *ACM SIGGRAPH, Practical physically-based shading in film and game production*, 2012.

[CB15]   Per Christensen and Brent Burley. Approximate reflectance profiles for efficient subsurface scattering. Technical Report 15-04, Pixar, 2015.

[CT81]   R. L. Cook and K. E. Torrance. A reflectance model for computer graphics. *Computer Graphics*, 15(3):307–316, 1981.

[dI11]   Eugene d'Eon and Geoffrey Irving. A quantized-diffusion model for rendering translucent materials. In *ACM Transactions on Graphics (TOG)*, volume 30, page 56. ACM, 2011.

[GQP15]   Jie Guo, Jinghui Qian, and Jingui Pan. Practical rendering of thin layered materials with extended microfacet normal distributions. In Jaakko Lehtinen and Derek Nowrouzezahrai, editors, *Eurographics Symposium on Rendering*. The Eurographics Association, 2015.

[Gul14]   Ole Gulbrandsen. Artist friendly metallic fresnel. *Journal of Computer Graphics Techniques Vol*, 3(4), 2014.

[HCJ13]   Ralf Habel, Per H Christensen, and Wojciech Jarosz. Photon beam diffusion: A hybrid monte carlo method for subsurface scattering. In *Computer Graphics Forum*, volume 32, pages 27–37. Wiley Online Library, 2013.

[Hei14]   Eric Heitz. Understanding the masking-shadowing function in microfacet-based brdfs. *Journal of Computer Graphics Techniques*, 3(2):32–91, 2014.

[JB02]   Henrik Wann Jensen and Juan Buhler. A rapid hierarchical rendering technique for translucent materials. *ACM Transactions on Graphics (TOG)*, 21(3):576–581, 2002.

[JdJM14]   Wenzel Jakob, Eugene d'Eon, Otto Jakob, and Steve Marschner. A comprehensive framework for rendering layered materials. *ACM Trans. Graph.*, 33(4):118:1–118:14, July 2014.

[JMLH01]   Henrik Wann Jensen, Stephen R. Marschner, Marc Levoy, and Pat Hanrahan. A practical model for subsurface light transport. In *Proceedings of the 28th Annual Conference on Computer Graphics and Interactive Techniques*, SIGGRAPH '01, pages 511–518, New York, NY, USA, 2001. ACM.

[KKCF13]   Alan King, Christopher Kulla, Alejandro Conty, and Marcos Fajardo. BSSRDF importance sampling. In *ACM SIGGRAPH 2013 Talks*. ACM, 2013.

[MPBM03]   Wojciech Matusik, Hanspeter Pfister, Matt Brand, and Leonard McMillan. A data-driven reflectance model. *ACM Transactions on Graphics*, 22(3):759–769, July 2003.

[PdMJ14]   Marios Papas, Krystle de Mesa, and Henrik Wann Jensen. A physically-based bsdf for modeling the appearance of paper. In *Computer Graphics Forum*, volume 33, pages 133–142. Wiley Online Library, 2014.

[Pol08]   Mikhail Polyanskiy. Refractive index database. http://refractiveindex.info, 2008. Accessed: 2015-08-03.

[Sch94]   Christophe Schlick. An inexpensive BRDF model for physically-based rendering. *Computer Graphics Forum*, 13(3):233–246, 1994.

[Vea97]   Eric Veach. *Robust monte carlo methods for light transport simulation.* PhD thesis, Stanford University, 1997.

[WMLT07] Bruce Walter, Stephen R. Marschner, Hongsong Li, and Kenneth E. Torrance. Microfacet models for refraction through rough surfaces. In *Proceedings of the Eurographics Symposium on Rendering*, 2007.